RESEARCH PAPER

Adsorption of Zinc Oxide Nanoparticles onto Esterified Carbonize Sago Hampas: Kinetic and Equilibrium Studies

E. K. Droepenu[1, 2*], B. S. Wee[1], S. F. Chin[1], K. Y. Kok[3] and E. A. Asare[1,2]

** kobladodzie01@yahoo.com*

Received: March 2020 Revised: July 2020 Accepted: October 2020

[1] Resource Chemistry Program, Faculty of Resource Science and Technology, Universiti Malaysia Sarawak, Kota Samarahan, Sarawak, Malaysia
[2] Graduate School of Nuclear and Allied Sciences, University of Ghana, AE1, Kwabenya-Accra, Ghana.
[3] Malaysian Nuclear Agency, Bangi, Kajang, Selangor, Malaysia

DOI: 10.22068/ijmse.17.4.152

Abstract: *Sago hampas was chemically modified through esterification to adsorb both laboratory and commercial synthesized Zinc oxide nanoparticles from water in a batch adsorption studies. The esterified sago hampas (ECSH) as a bio-sorbent was characterized using Energy-dispersive X-ray spectroscopy (EDX), Fourier-transform infrared spectroscopy (FT-IR), Scanning electron microscopy (SEM), Transmission electron microscopy (TEM), and Brunauer-Emmett-Teller (BET) technique. Investigating the effect of pH, contact time, initial sorbate ion concentration, temperature and sorbent mass were carried out where adsorption parameters were analyzed using Langmuir, Freundlich and Temkin models. The correlation between Kinetics of adsorption and the rate order of Zinc oxide nanoparticles on ECSH were also determined. The adsorption of Zinc oxide nanoparticles was found to increase with increasing contact time with the attainment of equilibrium at 100th minute with maximum removal efficiency of 85.5% (0.036 mg/g) and 89.6% (0.106 mg/g) for laboratory and commercial synthesized Zinc oxide nanoparticles from aqueous solution. An optimum pH of 8 with adsorbent dose of 2.0 g at a temperature of 50°C gave good results of Zinc oxide nanoparticles removal. The equilibrium data for both sorbate solutions fitted well for both Langmuir and Freundlich isotherm models. From the Langmuir model, ECSH recorded greater sorption capacity of 0.2 mg/g and 0.6 mg/g for laboratory and commercial synthesized Zinc oxide nanoparticles respectively. The kinetic studies showed pseudo-second order model as the best fitted for the sorption of Zinc oxide nanoparticles for both laboratory and commercial Zinc oxide nanoparticles.*

Keywords: *Esterified Sago hampas, Langmuir isotherm model, Freundlich isotherm model, Temkin isotherm model, Pseudo-first model, Pseudo-second model.*

1. INTRODUCTION

According to Lux research and Sargent [1, 2], Nano-industry is one of the fastest growing industries and about 17.8 billion dollars from public and private sector funding was invested into this sector. This has boosted the global socioeconomic value of nanotechnologies worldwide. From current literature reviews on potential hazardous effects of metal-containing nanoparticles, release of these nanoparticles (NPs) from different sources gets into different environmental media and pose a threat to target-and-non-target species such as algae, crustaceans, fish, bacteria, yeast, nematodes, protozoa and mammalian cells [3-6]. According to data adapted from Piccinno et al. [7], different nanoparticles are used in different products but Zinc oxide (ZnO) and Ag nanoparticles are the most commonly used in consumer products.
Although the potential hazard of high concentration of engineered nanoscale ZnO have been evaluated to some extent [8, 9], their toxicological data are rather sparse [10], although the toxicity of normal zinc and zinc compounds has been much reported [11, 12]. According to Malaysian Environmental Quality Act 1974, the maximum permissible limit of Zn in drinking water is 2.0 mg/l. Assessment in predicting the concentrations of engineered nanoparticles both in terrestrial and aquatic systems through simulated modelling experiments reported the concentrations of Ti, Ag and Zn nanoparticles as 10^{-8} -10, 10^{-8} -10^{-1} and 10^{-3} -10^{0} mg/kg respectively [13].
Much awareness of the environmental impact of metal ions in recent years has led to the enactment of strict legislation such as the Environmental Quality Act 1974, 1989 in Malaysia to attain the Sustainable Development Goal number 6 (SDG 6) [United Nations, 2016].

[DOI: 10.22068/ijmse.17.4.152]

Several methods, such as ion-exchange, chemical precipitation, reverse osmosis, electroflotation, ultrafiltration, or electrochemical deposition do not seem to be economically feasible nowadays due to their relatively high costs [14]. Therefore, adsorption which uses low cost materials with simple and effective method could be adopted. Many such materials used as sorbents include microbial biomass, Agricultural wastes, nanochitosan cellulose beads, sago waste, rice husk, coconut husk, clay, zeolites, biopolymers, metal oxides, microorganisms, sewage sludge, ash and activated carbon has been investigated to be very good for these metal ions [15-17].

In this study, sago hampas, a natural fibre from the sago plant mostly cultivated in Malaysia was chosen. The plant which is estimated to cover 45,000 hectares in Malaysia [18] after starch extraction, generates large tons of sago pith residue [19] which possess both air and water pollution when burnt or disposed into water bodies. This lignocellulose residue was suggested in its raw state to be a suitable and potential bio-sorbent [20] for heavy metal adsorption. The objectives of this study was to modify the sago hampas by a chemical process through esterification and then determine its effectiveness as sorbent on ZnO NPs in a batch adsorption studies through the variation of different factors such as pH, contact time, initial sorbate concentration, temperature and sorbent mass.

2. EXPERIMENTAL PROCEDURE

2.1. Materials

Wet Sago hampas was obtained from the sago industry in Mukah district, Sarawak state in Malaysia. The hampas was thoroughly washed with tap and deionized water to remove foreign particles and any inorganic material. The washed sample was air dried for two weeks at room temperature and then oven dried at 70 ˚C for 24 hours in order to obtain a biomass in a completely dried form. The dried sample was then ground into fine powder using blender (FGR-350) and screened through Retsch Analysensieb sieve mesh of size 210 μm (DIN-ISO 3310/1) on a mechanical shaker (Endecotts EFL 2 mk3 Test Sieve Shaker). The sieved sample was stored in zip-lock plastic bags to avoid moisture and fungal infection.

2.2. Chemical Processing of Adsorbent

About 100-200 g of the dried sieved sorbent sample was heated at a temperature range of 300-400 K in a muffled furnace (Protherm) for two hours. The charred sample was cooled at room temperature and nitrogen gas passed over it.

The charred sample was passed through an esterification process, a method reported by Wahi et al. [21] with some modifications. A weighed mass of 1:1 mass ratio of charred sago hampas sample and Hexadecanoic acid [$CH_3(CH_2)_{14}COOH$] was mixed with 50 ml of ethyl acetate ($CH_3COOC_2H_5$) in a round bottom flask with 7.5 ± 0.1 g of Calcium oxide added to quicken the process. The content was heated under reflux for 8 hours and the resulting mixture cooled at room temperature, filtered and washed with excess ethyl acetate and dried in a drying oven at a temperature of 50 ˚C. The dried esterified carbonized sago hampas (ECSH) was stored in a desiccator prior to analysis.

2.3. Characterization of Adsorbent

Samples of ECSH used before and after the batch adsorption studies were analyzed using different characterization techniques. FT-IR spectrum of the prepared ECSH samples were recorded using Thermo Nicolet iS10 spectrophotometer in the wave number range from 4000- 400 cm^{-1}. Morphology of ECSH was determined using Field Emission Scanning Electron Microscopy (Carl Zeiss GeminiSEM 500) with acceleration voltage of 10.0 kV, working distance of 11.6 mm and a chamber pressure of 40 Pa. The purity of elemental components of the sample was determined with EDX (JEOL 6390LA, Japan). Sample preparation for FE-SEM, EDX and FT-IR were carried out using method outlined by [22-24]. In addition, Brunauer-Emmett-Teller (BET) (Quantachrome, US Autosorb iQ,version 2.01) was used for the surface area determination. The sample was degassed at 175 ˚C for 2 hours [25] in a flowing N_2 gas and the N_2 absorption-desorption isotherms measured.

2.4. Sorbate Ion Preparation

ZnO (Commercial and Laboratory synthesized) nanocrystals with their physiochemical properties outlined in Table 1, were used for the batch adsorption studies. Sorbate preparation was carried out as per the procedure outlined by

[DOI: 10.22068/ijmse.17.4.152]

[24] with some modifications. ZnO NPs stock suspension of 1000 mg/l was prepared by dissolving 1.00 ± 0.1 g nanocrystalline powder of the commercial and laboratory synthesized samples each in 10 cm^3 volume of concentrated HNO_3, sonicated for 15 min at 20 KHz at an intensity of 200 W/L (Ney ULTRAsonik) and made up to the 1000 mg/l. A dilute concentration of 10 mg/l ZnO NPs solution was prepared from the stock from which serial dilutions of 0.2-1.0 mg/l were prepared and analysed spectroscopically using Atomic Absorption Spectrometer, AAS (iCE 3000 Series AA, Thermo Scientific). Air-acetylene was used as fuel at approximately 2300 ˚C and flowed at 0.9 L/min. Doubled-beam optics with monochromator reduced the detection limits and provided higher accuracy. The various parameters used for the AAS analysis is shown in Table 2. pH and conductivity of the sorbate solution was determined using PHS-W Series Benchtop pH/mV Meter and EUTECH COND 6^+. Prior to the adsorption studies, the solution was also analysed for particle characteristics in water by employing SEM and TEM techniques.

Table 1. Physiochemical properties of ZnO NPs used for the adsorption studies using ECSH

Parameter	Description and Properties
Commercial ZnO NPs	Particle size: <50 nm; BET: >97%; Surface area: >10.8 m^2/g; Density: 5.61 g/ml; 6% Al as dopant; Vendor: Sigma Aldrich.
Lab synthesized ZnO NPs	Synthesized from Zinc acetate dihydrate [$Zn(CH_3COO)_2{\cdot}2H_2O$] and potassium hydroxide [KOH] in a Solvothermal method of synthesis. Crystallite size: 11.0 nm; Morphology: Wurtzite hexagonal; Surface area: 59.90 m^2/g.

Table 2. AAS parameters used in the analysis of the synthesized ZnO samples.

Parameter	Characteristics
Wavelength (nm)	213.9
Flame type	Air-C_2H_2
Nebulizer uptake (s)	4
Burner height (mm)	14.2
Lamp current (%)	75
Rescale limit (%)	10
Standards (mg/L)	0.3000, 0.6000 and 1.000
Acceptable fit	0.995
Detection limit (mg/L)	0.0033

2.5. Batch Adsorption Studies

Adsorption efficiency of ECSH was investigated using batch studies by varying the pH, sorbent mass, contact time, initial sorbate concentration and temperature. All studies were carried out in a covered 250 ml Erlenmeyer flask containing 50 ml ZnO NPs solution on an electric hotplate magnetic stirrer (Fisherbrand) at a stirring speed of 240 rpm. The eluent taken was filtered using 0.45 µm filter paper and analyzed using AAS. All experiments were conducted in duplicates and two controls (adsorbent + distilled water and distilled water only) in order to estimate the amount of any ZnO NPs that might be present in the sorbent.

Kinetic study experiments were carried out by adding 0.5 ± 0.1 g of ECSH to 50 ml of 0.3 mg/l ZnO NPs solution at a pH of 6 in the closed Erlenmeyer flask and stirred for 150 min at 30 ˚C and a speed of 240 rpm. Aliquots of the filtrate solution were taken at predetermined intervals of 20-150 minutes for the analysis of the residual NPs concentration in the solution. The effect of pH was also studied by varying the sorbate solution between 2 to 13 with a fixed sorbent mass of 0.5 ± 0.1 g whiles the temperature and stirring speed at 30± 2 ˚C and 240 rpm for sixty (60) minutes respectively were maintained. However, the effect of initial sorbate concentration and contact time was carried out by keeping the temperature, pH, sorbent mass and stirring speed at 30± 2 ˚C, 6, 0.5± 0.1 g and 240 rpm respectively. The experimental conditions used in the study are illustrated in Table 3. Percentage removal as well as the amount of sorbate NPs adsorbed (mg) onto the adsorbent per unit mass (g) at the required contact time, q_e (mg/g) was calculated using the equation:

$$\text{Removal}(\%) = \frac{(C_O - C_e)}{C_O} \times 100 \quad (1)$$

$$q_e = \frac{(C_O - C_e)/V}{W} \quad (2)$$

Where, C_o and C_e (mg/l) are the concentrations of sorbate NPs at initial and equilibrium contact time, respectively. V is the volume of the solution (L) and W is the mass of adsorbent used (g).

[DOI: 10.22068/ijmse.17.4.152]

Table 3. Experimental conditions for batch adsorption for Zn (II) removal using ECSH.

Experimental conditions	Variations
Initial sorbate ion conc, (mg/l)	
Lab synthesized	0.09, 0.23, 0.42, 0.57, 0.80
Commercial synthesized	0.41, 0.84, 1.01, 1.03, 1.18.
Sorbate mass (g)	0.50, 1.0, 1.5, 2.0, 2.5.
pH	2, 5, 8, 10, 13.
Contact time (min)	20, 40, 60, 80, 100, 120, 150
Temperature	25, 30, 40, 50, 60, 70.

2.6. Adsorption Isotherm

The sorption equilibrium data of Zn (II) on ECSH was analyzed in terms of three models; Langmuir, Freundlich and Temkin isotherms.

The assumption for Langmuir isotherm model is that, finite number of active sites are distributed homogeneously over the surface of the sorbent with the same affinity for adsorption. The equation as proposed by [26] is expressed as;

$$\frac{1}{q_e} = \left[\frac{1}{Q_O K}\right]\frac{1}{C_e} + \frac{1}{Q_O} \quad (3)$$

Where, C_e- equilibrium concentration, mg/g, q_e- amount absorbed at equilibrium, mg/g, Q_o and K- Langmuir constants relating to adsorption capacity and energy of adsorption which were determined from the slope and intercept of the linear plot of $1/q_e$ Vs. $1/C_e$. The essential features of a Langmuir isotherm can be expressed in terms of a dimensionless constant separation factor or equilibrium parameter, R_L that is used to predict if an adsorption system is "favorable" or "unfavorable". The separation factor, R_L is defined by [27] and represented with the Equation:

$$R_L = \frac{1}{1 + KC_O} \quad (4)$$

Where, C_o- sorbate concentration, mg/l, K- Langmuir adsorption equilibrium constant, L/g. The isotherm is unfavorable when $R_L>1$, the isotherm is linear when $R_L=1$, the isotherm is favorable when $0<R_L<1$ and the isotherm is irreversible when $R_L=0$.

Freundlich isotherm model applies to adsorption on heterogeneous surfaces with interaction between the adsorbed molecules but not restricted to the formation of a monolayer. The model assumes that as the sorbate concentration increases, its concentration on the sorbent surface also increases and, correspondingly, the sorption energy exponentially decreases on completion of the sorption centers of the adsorbent. The equation relating to this model proposed by [28] is:

$$\log q_e = \log K_f + \frac{1}{n}\log C_e \quad (5)$$

Where, q_e- amount adsorbed at equilibrium, mg/g, C_e- equilibrium concentration, mg/l, K_f and n- Freundlich model constants. These constants can be obtained from the slope and intercept of the plot of log q_e against log C_e.

Temkin isotherm assumes that, the fall in heat of sorption is linear rather than logarithmic, as implied in the Freundlich equation. The isotherm model relates the Equation proposed by [29]:

$$q_e = B_T \ln A_T + B_T \ln C_e \quad (6)$$

Where, $B_T = (RT/b_T)$, q_e- amounts adsorbed at the equilibrium concentration, mg/g, C_e- amounts adsorbed at the equilibrium concentration, mg/l, T- absolute temperature, K, R- universal gas constant, 8.314˚J/(mol K). The constant b_T is related to the heat of adsorption [30, 31].

2.7. Adsorption Kinetics

The adsorption constant rate of Zn (II) on ECSH was derived from the pseudo-first order (Equ. 7) and pseudo-second order (Equ.8) sorption equations [32];

$$\log(q_\theta - q_t) = \log q_\theta - \frac{k_1 t}{2.303} \quad (7)$$

Where, k_1 (min^{-1})- rate constant of the pseudo-first order sorption, q_t (mg/g)- amount of ZnO NPs adsorbed by ECSH at time t (min) and q_θ (mg/g)- amount of ZnO NPs adsorbed at equilibrium. The fairly linear plots of log ($q_\theta - q_t$) versus t confirms the applicability of the above equation for ZnO NPs onto ECSH. The value of k_1 was calculated from the slope of this linear plot.

$$\frac{t}{q_t} = \frac{1}{k2q_\theta^2} + \frac{t}{q_\theta} \quad (8)$$

Where, k_2 (g/mg min^{-1}) is the rate constant. k_2 and q_θ can be obtained from the intercept and slope of plotting of t/q_t versus t.

[DOI: 10.22068/ijmse.17.4.152]

3. RESULTS AND DISCUSSION

3.1. Characterization

The FT-IR spectral details of ECSH before and after ZnO NPs adsorption is illustrated in Fig. 1 (a) and (b). Broad peak at 3589.56 cm^{-1} and 3011.61 cm^{-1} correspond to the presence of intermolecular hydrogen bonded O-H stretching modes [33-34] before the adsorption studies. After the experiment where the ZnO NPs were loaded onto the sorbent, the later peak shifted to 3019.20 cm^{-1} whereas the former diminished. The dried sorbent used for the after-sorption analysis was taken from the study where the initial sorbate concentration, pH and reaction time were 0.3 mg/L, 6 and 60 minutes respectively. The shift in the band at 2791.82 cm^{-1} to 2787.83 cm^{-1} in the IR spectrum (- C- H stretching) could be associated with the presence of alcohols, fatty acids, aldehydes, ketones and n-alkyl esters, present in the lignocellulose sorbent [35-36]. An infrared spectrum pattern of Adulsa leaf powder (Justicia adhatoda), orange peel, Hogla leaves (Typha elephantine Roxb), and sago wastes, show similar spectrum of band between 2891-2900 cm^{-1} being suggested to the –C-H stretching of -CH_2 and -CH_3 in their study.

Peak bands appearing at 1690.73 and 1413.30 cm^{-1} are indicative of the presence of C=O stretching in carboxylic and N=O bending in nitro groups respectively which shifted to sharp bands at 1704.30 and 1400.68 cm^{-1} respectively. Also, sharp peak observed at 1211.89 cm^{-1} was assigned to C–O stretching in ethers and acetyl group associated with the presence of cellulose, hemicellulose and lignin or the ethyl acetate [35, 37] but seldom shifted to a weak peak at 1217.55 cm^{-1} after the studies.

The shifting of these bands is an indicative of the ZnO NPs been adsorbed on the active sites of ECSH adsorbent [38-39]. Proof of ZnO NPs attachment onto the surfaces of the ECSH adsorbent was clearly evidenced from the appearance of a smooth surfaces of the adsorbent in the SEM morphology (inset).

3.2. SEM Analysis

The surface morphology of ECSH and ZnO NPs-loaded ECSH analyzed using JEOL JSM-6390LA model are illustrated in figure 2.

SEM micrograph reveals significant changes on the surface morphology of the sorbent both before and after the adsorption process. The rough and heterogeneous surface nature of ECSH before adsorption predicts a high probability of active sites for the attachment of the NPs [40]. The uptake of ZnO NPs onto ECSH (Fig. 2b) reveals a change in morphology of the sorbent's surface been smooth. This is as a result of the NPs acting as a bridge connecting the active sites to form a uniform surface structure [41]. The dried sorbent

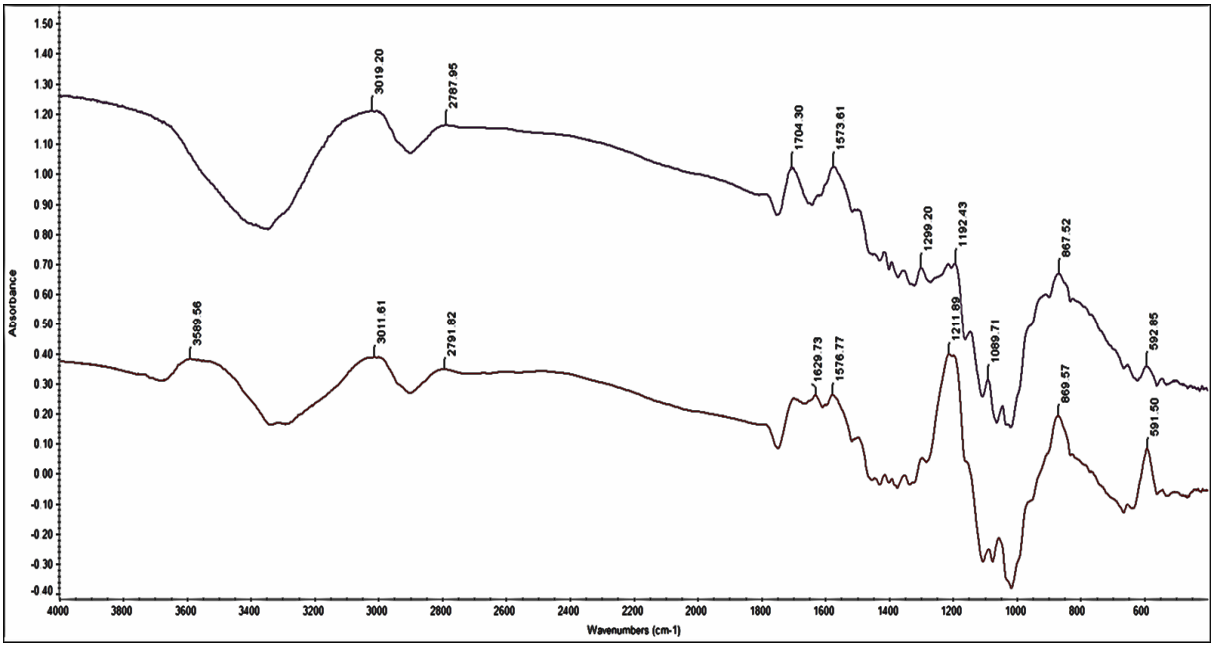

Fig. 1. FT-IR spectrum of (a) ECSH before and (b) ECSH after adsorption studies.

[DOI: 10.22068/ijmse.17.4.152]

used for the after-sorption SEM analysis was taken from the study where the initial sorbate concentration, pH and reaction time were 0.3 mg/L, 6 and 60 minutes respectively.

The SEM and TEM micrographs of the nanocrystalline ZnO powders used for the sorbate solution shown in Fig. 3 are made of wurtzite and rod-like structures for laboratory and commercial synthesized samples. On the other hand, the laboratory synthesized samples appear to be agglomerated whereas the commercial samples are not.

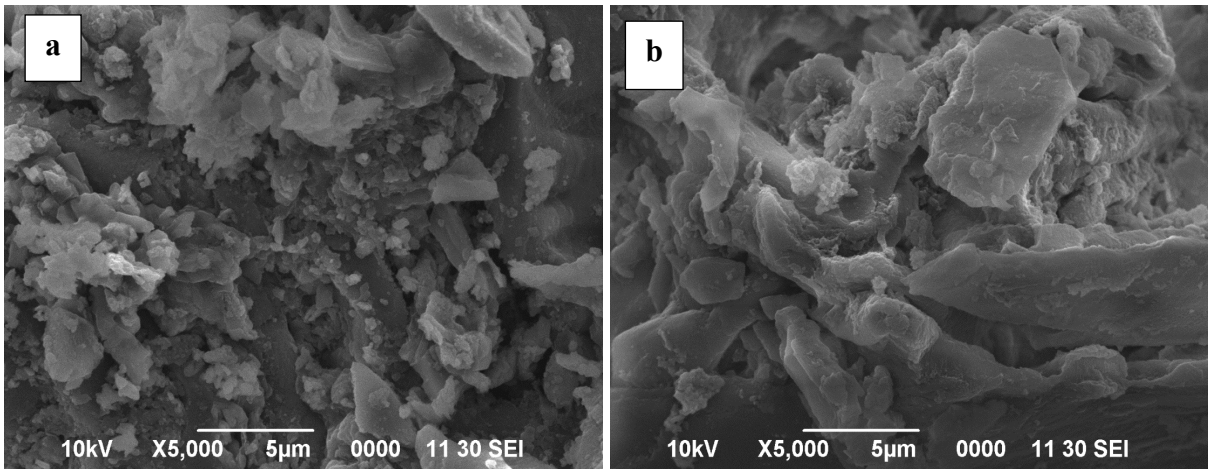

Fig. 2. SEM micrograph details of (a) ECSH before adsorption (b) Zn (II)-ECSH loaded after adsorption studies.

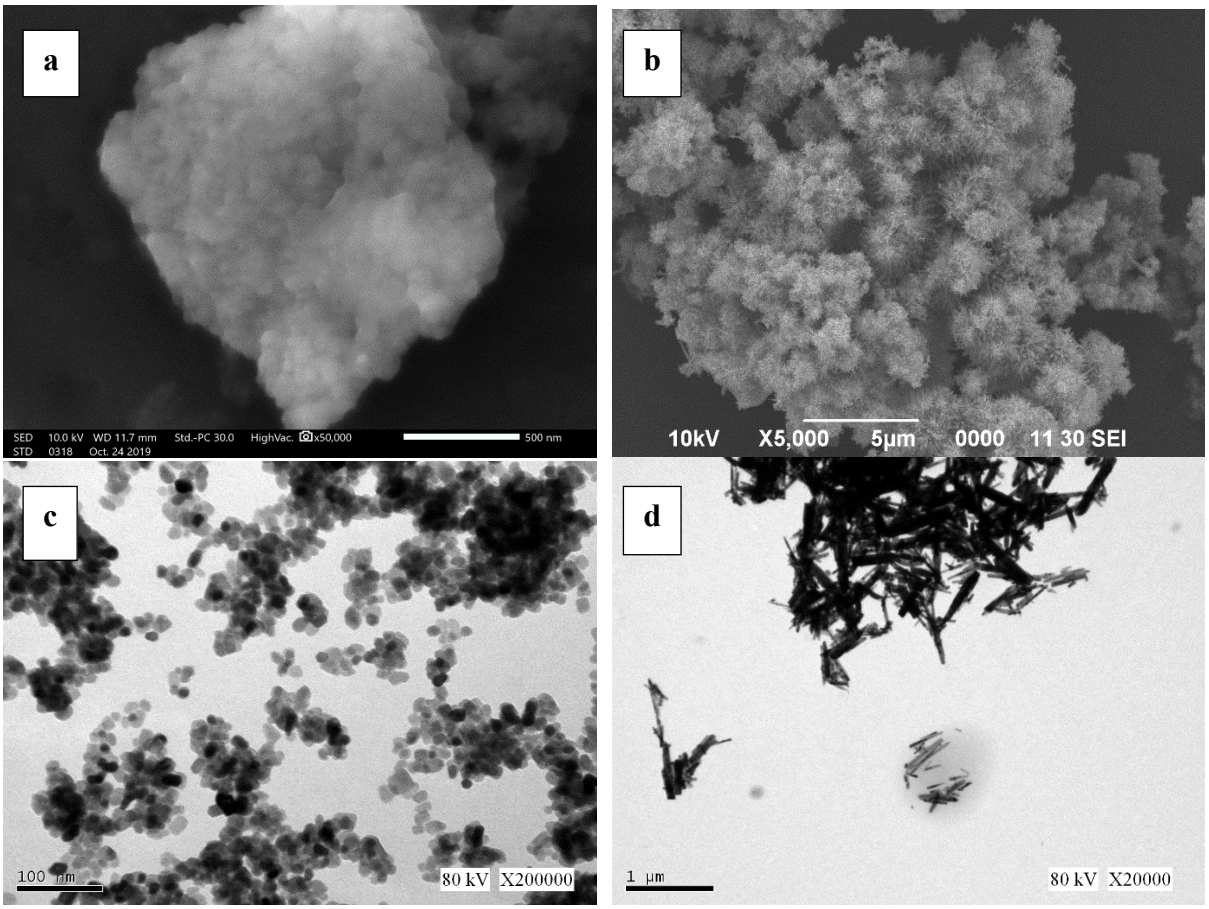

Fig. 3. SEM micrograph of nanocrystalline ZnO powders from (a) laboratory (b) commercial synthesis and TEM images of nanocrystalline ZnO powders from (c) laboratory (d) commercial synthesis prior to the adsorption studies.

[DOI: 10.22068/ijmse.17.4.152]

3.3. EDX Analysis

The EDX spectra for the two nanocrystalline ZnO powders as well as ECSH (before and after adsorption studies) are illustrated in Fig 4. The ECSH sorbent used for the after-sorption analysis was taken from the dried sample prepared from the study where the initial sorbate concentration, pH and reaction time were 0.3 mg/L, 6 and 60 minutes respectively. As observed from the spectra, the ZnO samples are basically made up of elemental zinc and oxygen (Zn & O), although Al was used as a dopant according to the manufacturer this was invisible in the EDX analysis. This could be due to the insignificant amount which the equipment could not detect. However, the sorbent, ECSH was composed of elemental carbon and oxygen and zinc (C, O & Zn) with different percentage masses.

3.4. BET Analysis

The BET surface area of ECSH determined from the isotherm plot as shown in Fig 5 was found to be 5.52 m^2/g, average pore size of 1.67 $\times 10^2$ Å and pore volume of 4.60 $\times 10^{-2}$ cm^3/g. Though the surface area tends to be small, the multiple functional groups from the chemicalization of the sorbent enhanced the adsorption capacity.

3.5. Effect of pH

The study carried out at different pH (2-13) shows a change in the % removal of ZnO NPs as shown in the Fig 6. The change in pH as a result of the influence of the H^+ and OH^- ions on the surface chemistry [42-43] of ECSH mostly affected the uptake of NPs through hydrogen bonding and ion exchange mechanisms [44] as illustrated in the chemical reaction below;

- Hydrogen bonding:

$$2(\text{-R-OH}) + M(OH)_2 \rightarrow (\text{-R-OH})_2 \text{ ----- } M(OH)_2 \quad \text{(I)}$$

- Ion exchange:

$$2(R - OH) + M^{2+} \rightarrow 2(R - OM) + 2H^+ \quad \text{(II)}$$

$$2(R - OH) + M^{2+}\ 2OH^- \rightarrow 2(R - OM) + 2H_2O \quad \text{(III)}$$

Conversely, since dissolution of the ZnO NPs decreases at higher pH according to [45], more NPs are present in the solution which are adsorbed onto ECSH surfaces either by adsorption or sedimentation as reported by [46]. In all these mechanisms, the functional groups on the sorbent surface interact with these particles through weak Van der Waals force of attractions to form coordinate compounds or chelate compound [45].

From Fig.6, the maximum adsorption occurred at pH 8 with % Zn (II) ion removal of 85.6% and 88.1% for laboratory and commercial synthesized ZnO NPs respectively. However, the concentration eventually decreased to 82.2% and 84.3% at pH 13. The reason being that, at low pH of 2, protonation of active sites (–OH functional group as indicated from FT-IR analysis) competes with Zn (II) ions due to high electrostatic repulsion, hence lower % removal of Zn (II) ions. But, as pH increased to an optimum level of 8, the concentration of H^+ decreases, rendering an increase in the negative charge density of ECSH surface to facilitate enough binding of Zn (II), thereby resulting in the maximum removal [47-48]. Beyond the optimum pH value, a decrease in uptake of the Zn (II) ions was observed as a result of the precipitation of metal hydroxide species, $Zn(OH)_2$ competing with the Zn (II) ions for the active site for attachments [49]. Besides, agglomeration of the laboratory synthesized ZnO NPs also contributed to the difference in the uptake of the two sorbate ions. The higher the agglomeration, the fewer the uptake as few bigger particles tend to occupy most active sites of the sorbent. When this study was compared to a study by [17,46], the optimum pH at which Zn (II) and ZnO NPs were adsorbed onto raw sago waste and activated carbon were at a pH of 9 and 8 respectively.

3.6. Effect of Adsorbent Mass

In this study, five sorbent masses (0.5-2.5 g) were selected in 50 ml of 0.30 mg/l ZnO NPs solution with pH of 6, agitated at 240 rpm and at a temperature of 30 ^oC. The % ZnO NPs removal as well as the adsorption efficiency of ECSH are presented in Fig. 7.

[DOI: 10.22068/ijmse.17.4.152]

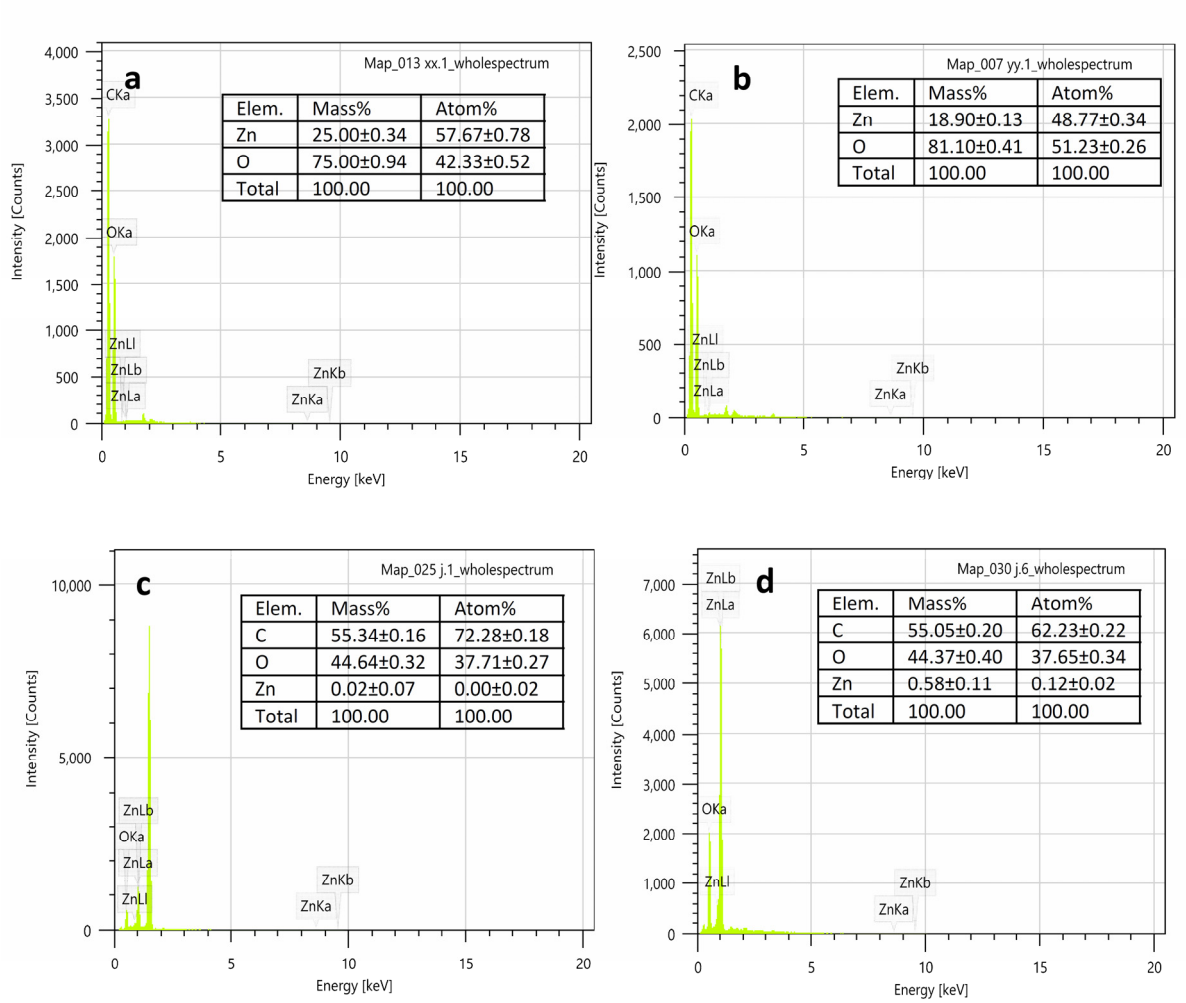

Fig. 4. EDX spectra of (a) laboratory nanocrystalline ZnO NPs (b) commercial nanocrystalline ZnO NPs (c) ECSH before (d) Zn (II)-ECSH loaded after adsorption studies.

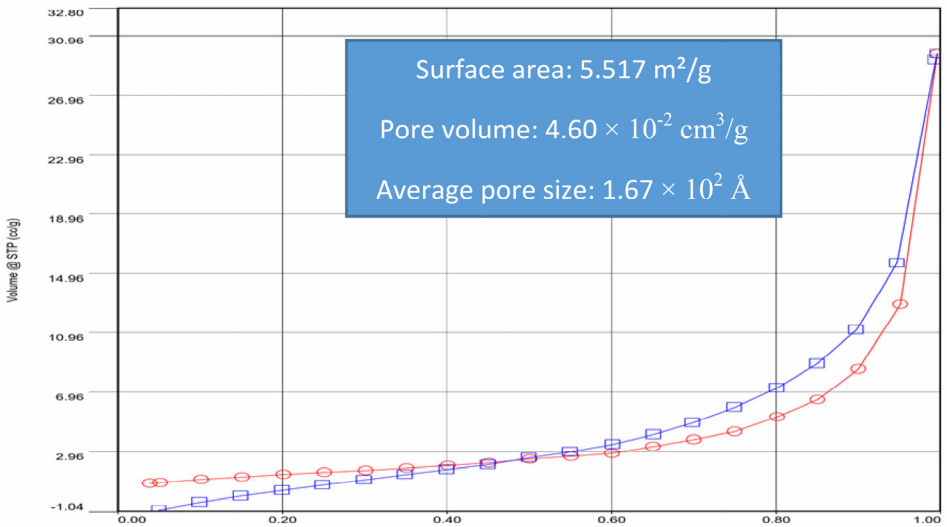

Fig. 5. N_2 adsorption- desorption isotherms of ECSH sorbent

[DOI: 10.22068/ijmse.17.4.152]

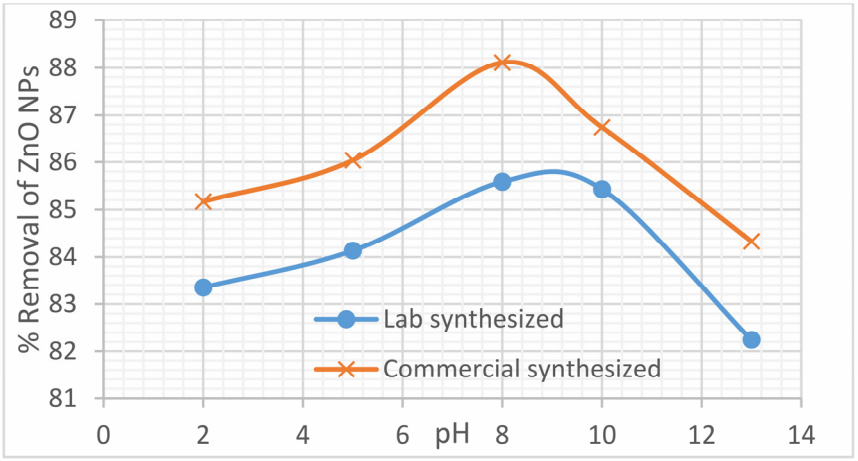

Fig. 6. Effect of pH on ZnO NPs bio-sorption by ECSH using 0.30 mg/l of sorbate solution at 240 rpm and 30 ˚C.

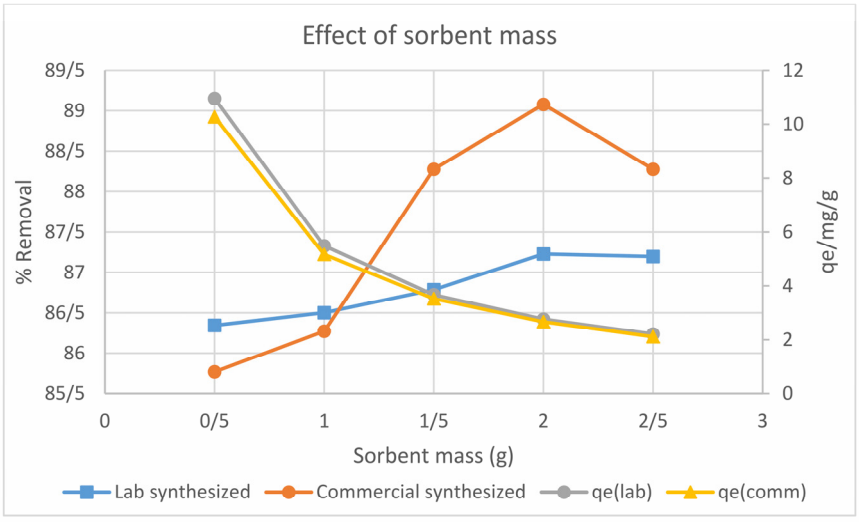

Fig. 7. Effect of sorbent mass on ZnO NPs bio-sorption removal and adsorption efficiency of ECSH using 0.30 mg/l of sorbate solution at pH 6, 240 rpm and 30 ˚C.

The result obtained clearly indicates an increase in the % ZnO NPs removal (87.2% and 89.1% for laboratory synthesized and commercial synthesized Zn NPs respectively) at an optimum dosage of 2.0 g, beyond which the removal efficiency became constant in the case of the lab synthesized but a decrease in the case of the commercial synthesized sample. Contrary to this, the adsorption efficiency decreased for both sorbate solutions from 10.9 - 2.2 mg/g and 10.2 – 2.1 mg/g. The initial increase was mainly due to the greater availability of more binding sites for complexation [50-52]. On the other hand, as the sorbent mass increases at constant concentration and volume of sorbate solution, the available total surface area of ECSH became unsaturated, and ZnO NPs are inadequate to cover all active sites, thereby decrease in the equilibrium efficiency [53-55]. Also, decreases in the sorption efficiency could be attributed to the overlapping of sorbent active sites (screening effect of a dense outer layer of cells of the sorbent) which blocks the binding sites from NPs [52, 56-57].

3.7. Effect of Contact Time

The effect of initial sorbate concentration against contact time on the removal of ZnO NPs was studied by varying the time of contact from 20 min to 150 min and the observed results are presented in Fig.8.

[DOI: 10.22068/ijmse.17.4.152]

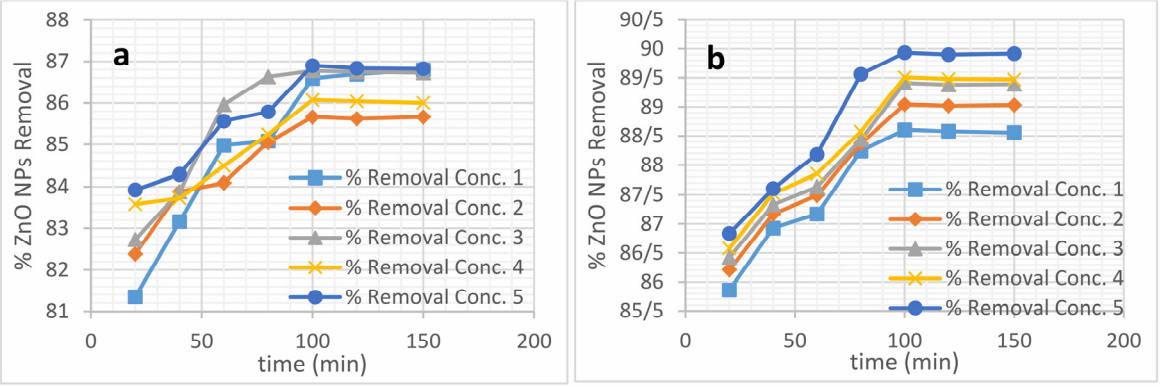

Fig. 8. Effect of initial concentration and time on the sorption of (a) Laboratory (b) Commercial synthesized Zn (II) bio-sorption by ECSH at pH 6, 240 rpm and 30 ˚C.

From the experimental result, a rapid uptake of ZnO NPs ions was observed within the first 20 min until equilibrium was attained at the 100th min with maximum % removal of approximate 86.5% and 89.6% for both laboratory and commercial synthesized ZnO NPs. The removal efficiency of ZnO NPs increased from 0.008 mg/g to 0.036 mg/g for laboratory synthesized ZnO NPs whereas that of commercial synthesized ZnO NPs also increased from 0.035 mg/g to 0.106 mg/g. However, after the equilibrium point at the 100th minute, there was no significant increase in the rate of removal for both synthesized NPs. The rapid increase in NPs removal at the initial stages was mainly due to the more number of available active sites on its surface area and is normally controlled by diffusion process from the bulk to the surface [58]. But beyond the equilibrium point, the adsorption sites get exhausted and thus attained equilibrium leading to minimal decrease in the ZnO NPs removal [59].

3.8. Effect of Temperature

Fig.9 illustrates the effect of temperature on the adsorption of ZnO NPs onto ECSH at varying temperatures between 25ºC - 70ºC while keeping the other parameters constant.

The observed result presented in Fig. 9 indicates an increase in ZnO NPs uptake (85.1% to 86.8% and 85.4% to 89.9% for laboratory and commercial ZnO respectively) as the temperature increased from 25 ˚C to 50 ˚C, but thereafter shows a decrease. The initial increase could be attributed to the increased mobility of NPs leading to their acceleration towards the active site of the sorbent. This eventually increased their removal percentage [60]. But beyond the 50 ˚C temperature, there was a decrease in the % removal due to the weakening of the binding forces existing between the NPs and active sites present on the surface of the sorbent [61]. It might also be due to fiber attrition with respect to temperature increase [62]. The significant percentage difference between the two ZnO NP sources could be attributed to the aggregation nature of the samples amounting to the particle size. According to [63], surface area of a particle is a function of the particle's size. Therefore, larger particle size decreases metal adsorption whereas a smaller particle size increases the metal adsorption.

3.9. Adsorption Isotherm

Langmuir, Freundlich, and Temkin, isotherms were applied to describe the affinity and distribution of sorbate molecules on the sorbent surface at equilibrium. The experimental data for adsorption isotherm for the two synthesized ZnO NPs are shown in Table 4a & 4b.

The Langmuir, Freundlich and Temkin isotherm plots for laboratory and commercial synthesized ZnO NPs are represented in Fig.10, 11 & 12. Considering their R^2 values which are 0.997 & 0.990, 0.999 & 0.998 and 0.905 & 0.993 respectively, it suggests that all the three models fit the study but Langmuir and Freundlich isotherms fit best confirming the applicability of the model. The fact that the data fits well may be due to the homogeneity of active sites distribution of the ECSH. This result is in agreement with investigations carried out on the sorption efficiency of both raw and chemically modified sago waste on copper, zinc, and lead by [17, 21, 64-66].

The constant parameters, regression correlation coefficient (R^2) and separation factors calculated for the three isotherm models are tabulated in Table

[DOI: 10.22068/ijmse.17.4.152]

5a & 5b. The calculated adsorption capacity, Q_o, according to Langmuir model for ECSH at 30 ˚C are 0.250 mg/g and 0.690 mg/g for the two sorbate solutions. This presupposes that, the potential for the sorbent to remove commercial synthesized ZnO NPs from aqueous solution was higher than laboratory synthesized ZnO NPs. The calculated R_L values for this isotherm model for both sorbates solutions on ECSH at different concentrations were between 0 and 1 indicating favorable adsorption of ZnO NPs in this study.

Also, the calculated Freundlich model constant 'n' for both synthesized ZnO NPs falls between 0 and 10 suggesting a relatively strong sorption of the sorbate ions onto ECSH. This is an indication of an enhancement of electrostatic force (Van der Waal's) between the sorbent surface and the sorbate ions.

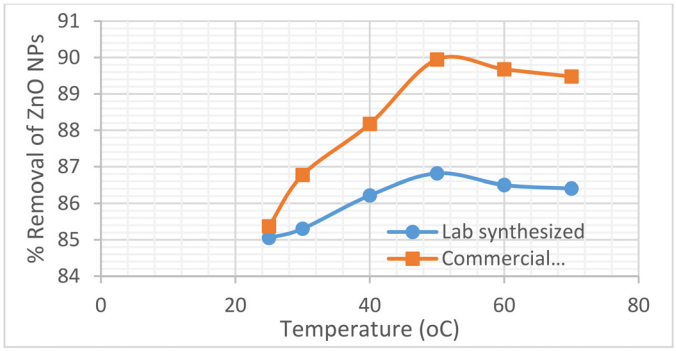

Fig. 9. Effect of Temperature on ZnO NPs bio-sorption by ECSH 0.3 mg/l of sorbate solution at pH 6 for 60 min.

Table 4. a) Experimental data for adsorption isotherm for lab synthesized Zn (II) solution at 30 ˚C, pH at 6, for 60 min at 240 rpm.

Initial Conc. [C_o], (mg/l)	Equil. Conc. [C_e], (mg/l)	Amount absorbed at Equil. [q_e], (mg/g)
0.092	0.014	0.009
0.229	0.036	0.019
0.418	0.069	0.035
0.566	0.096	0.047
0.800	0.138	0.066

Table 4.b) Experimental data for adsorption isotherm for commercial synthesized Zn (II) solution at 30 ^oC, pH at 6, for 60 min at 240 rpm.

Initial Conc. [C_o], (mg/l)	Equil. Conc. [C_e], (mg/l)	Amount absorbed at Equil. [q_e], (mg/g)
0.412	0.048	0.036
0.843	0.105	0.074
1.01	0.129	0.088
1.03	0.134	0.089
1.18	0.158	0.102

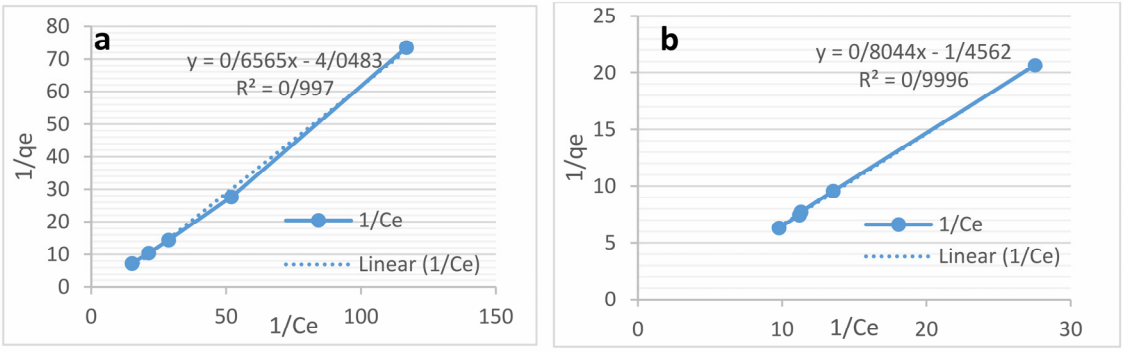

Fig. 10. Langmuir isotherm plot for (a) laboratory and (b) commercial synthesized ZnO NPs solutions.

[DOI: 10.22068/ijmse.17.4.152]

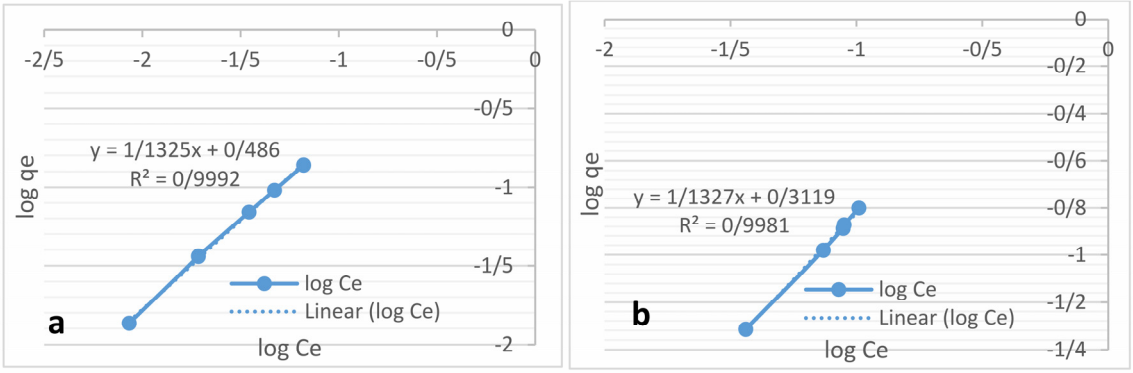

Fig. 11. Freundlich isotherm for (a) laboratory and (b) commercial synthesized ZnO NPs solutions.

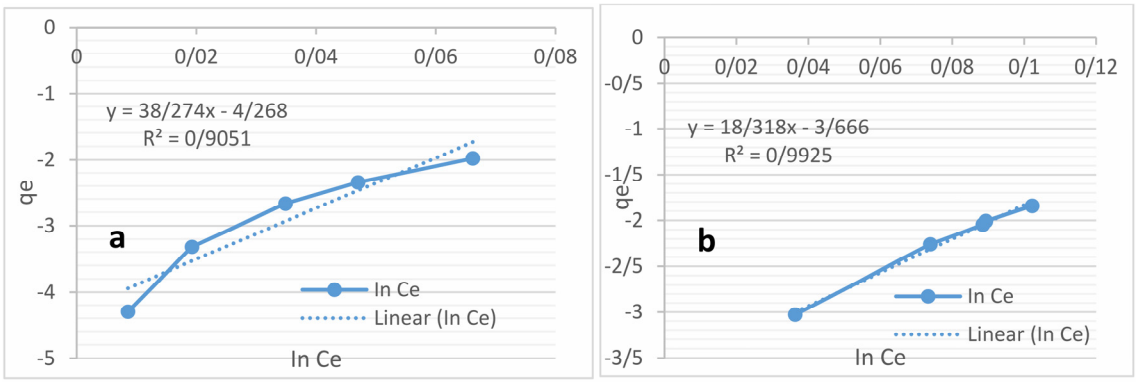

Fig. 12. Temkin isotherm for (a) laboratory and (b) commercial synthesized ZnO NPs solutions.

Table 5. a) Constant parameters and correlation coefficient (R^2) for lab and commercial synthesized ZnO NPs solution at 30 ˚C, pH at 6, for 60 min at 240 rpm

Parameters	Lab synthesized ZnO NPs	Commercial synthesized ZnO NPs
Langmuir isotherm		
Q_o [mg/g]	0.247	0.687
K, [L/g]	6.167	1.810
R^2	0.997	0.999
Freundlich isotherm		
K_f, [L/g]	0.327	0.488
n	0.883	0.883
R^2	0.999	0.998
Temkin isotherm		
A_T, [L/g]	1.12	1.22
B_T	38.27	18.32
b_T	65.82	137.52
R^2	0.905	0.993

[DOI: 10.22068/ijmse.17.4.152]

Table5. b) Separation factors calculated for lab and commercial synthesized ZnO NPs solution at 30 ˚C, pH at 6, for 60 min at 240 rpm

$[C_o]$ lab synthesized ZnO NPs (ppm)	R_L. lab synthesized ZnO NPs	$[C_o]$ commercial synthesized ZnO NPs (ppm)	R_L. commercial synthesized ZnO NPs
0.092	0.638	0.412	0.573
0.229	0.415	0.843	0.396
0.418	0.280	1.01	0.353
0.566	0.223	1.03	0.350
0.800	0.169	1.18	0.319

3.10. Adsorption Kinetics

In order to understand the interactions between the targeted ZnO NPs and the ECSH sorbent, a plot of log (q_e-q_t) vs t and t/q_t vs t for pseudo-first order and pseudo-second-order reaction of the adsorption of both laboratory and commercial synthesized ZnO NPs are illustrated in Figs. 13 and 14. Also the calculated rate constants (k_1, k_2, q_e) and their corresponding regression coefficient values (R^2) are presented in Table 6.

The correlation coefficients for pseudo-second-order for the two sorbate solutions at the different initial concentrations are better represented than the pseudo-first order model. However, its estimated q_e values are far below the theoretical values as presented in Table 6. Moreover, the calculated q_e values of the first order model gave quite close values to the experimental values at the various initial ZnO sorbate solutions except for commercial synthesized ZnO NPs with concentrations of 1.03 mg/l and 1.18 mg/l. Fig 15 compares the theoretical and experimental q_e values for both laboratory and commercial synthesized ZnO NPs. This study is in agreement with a previous work reported by [17] where metal zinc ion adsorbed onto raw sago waste showed a pseudo-second order.

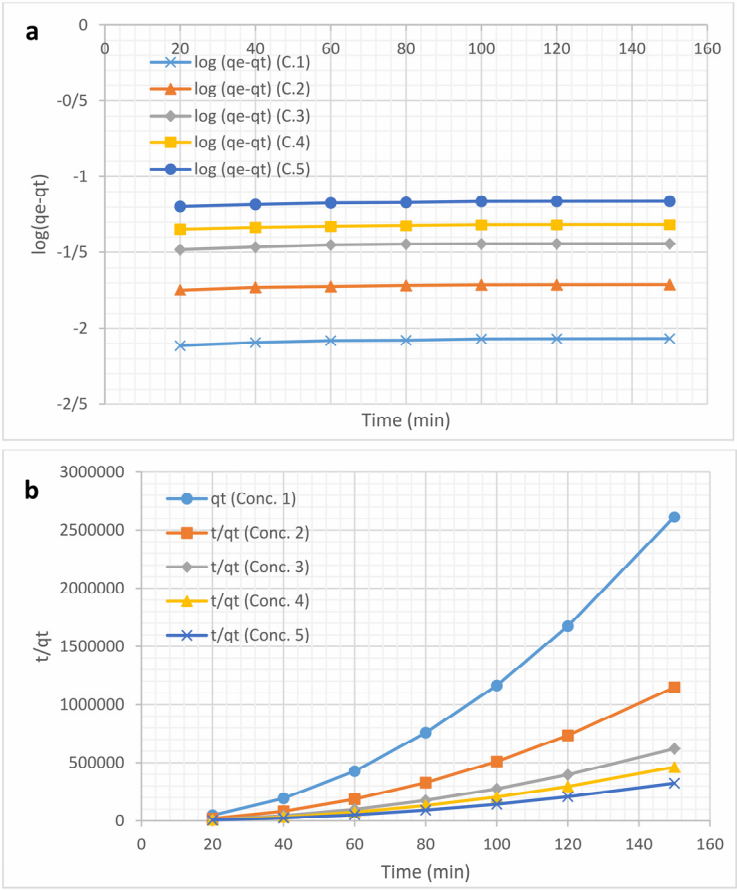

Fig. 13. (a) Pseudo-first (b) Pseudo-second kinetic plot for the adsorption of laboratory synthesized ZnO NPs onto ECSH.

[DOI: 10.22068/ijmse.17.4.152]

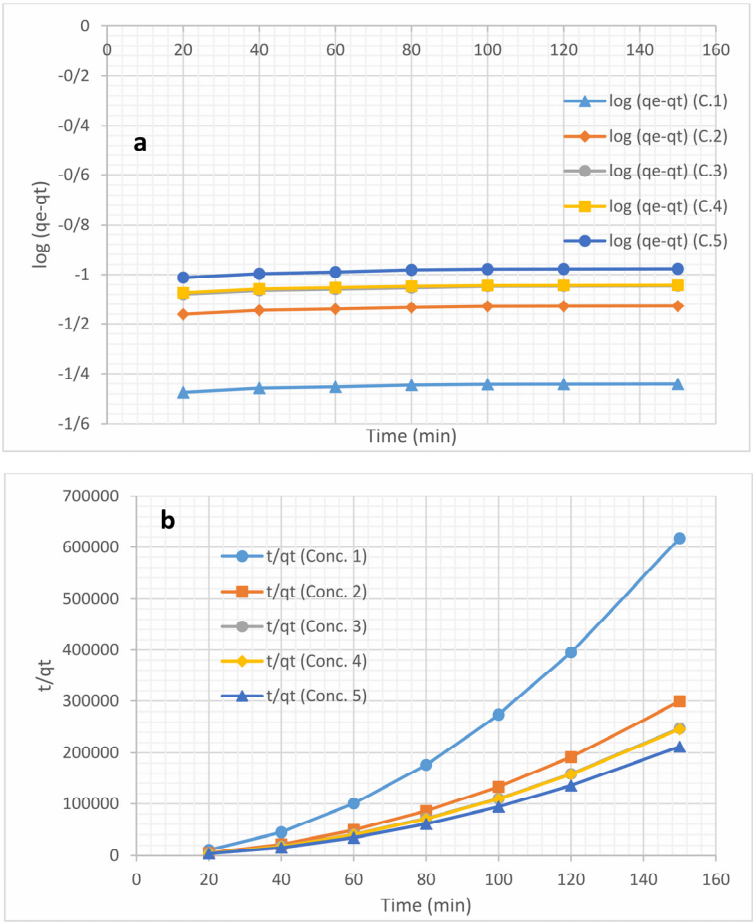

Fig. 14. (a) Pseudo-first (b) Pseudo-second kinetic plot for the adsorption of commercial synthesized ZnO NPs onto ECSH.

Table 6. Rate constants and regression correlation coefficient (R^2) for Lab synthesized (Lab synt) and commercial synthesized (Com synt) ZnO NPs solution at 30 ˚C, pH at 6, for 60 min at 240 rpm.

Initial conc, C_o [mg/l]	Pseudo-first order			Pseudo-second order			
	$q_{e.theo.}$ (mg/g)	k_1 (min^{-1})	R^2	$q_{e.exp}$ (mg/g)	$q_{e.theo}$ (mg/g)	k_2 (g/mg.min)	R^2
Lab synt.							
0.092	0.009	6.91e-4	0.808	0.008	5.12e-5	1.69e-6	0.950
0.229	0.018	6.91e-4	0.788	0.019	1.16e-4	3.71e-6	0.949
0.418	0.033	6.91e-4	0.728	0.036	2.15e-4	6.86e-6	0.949
0.566	0.045	4.61e-4	0.842	0.048	2.89e-4	9.23e-6	0.940
0.800	0.064	6.91e-4	0.825	0.069	4.12e-4	3.86e-5	0.950
Com.synt.							
0.412	0.034	4.61e-4	0.778	0.036	2.16e-4	6.89e-6	0.949
0.843	0.068	4.61e-4	0.806	0.074	4.46e-4	1.42e-5	0.949
1.014	0.084	6.91e-4	0.832	0.090	5.39e-4	1.72e-5	0.950
1.028	0.085	4.61e-4	0.767	0.091	5.42e-4	1.73e-5	0.949
1.180	0.098	6.91e-4	0.804	0.105	6.30e-4	2.01e-5	0.949

[DOI: 10.22068/ijmse.17.4.152]

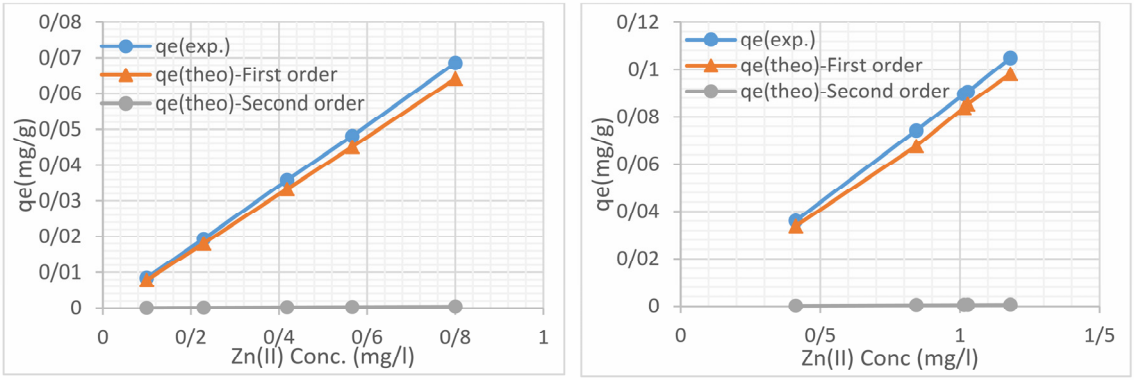

Fig. 15. Comparison between the experimental ($q_{e.exp}$) and calculated ($q_{e.theo}$) data for adsorption of ZnO NPs onto ECSH at 30 ˚C.

4. CONCLUSION

The study confirms successful esterification process of the sago hampas with functional groups such as hydroxyl, carboxyl and nitro groups confirmed by FTIR characterization. The process yielded a surface area of 5.52 m^2/g with average pore size and volume 1.67 × 10^2 Å and 4.80 × 10^{-2} cm^2/g. However, the morphology of the sorbate ions in solution had some slight influence on the sorption capacity of the sorbent as uptake of agglomerated particles in the laboratory synthesized onto ECSH were lesser as compared to the smaller rod-like particles of the commercial synthesized ZnO. The 100^{th} minute was observed as the optimum contact time for ECSH to remove 85.5% (0.036 mg/g) and 89.6% (0.106 mg/g) laboratory and commercial synthesized ZnO NPs from aqueous solution. The optimum sorbent mass for maximum NPs removal was 2.0 g at pH of 8. The adsorption isotherms were well fitted by the Langmuir and Freundlich models with strong adsorption and the process was best described by pseudo-second-order model. However, the esterified lignocellulose sorbent material (ECSH) used in this study could help alleviate the pollution effect of water bodies with these nanoparticles that are very difficult to eliminate due to their sizes. The study saw an improvement of sorption efficiency of about 25% from the raw sago used in the sorption of Zn^{2+} ions in a study by Wahi et al., 2010.

ACKNOWLEDGMENT

The authors acknowledge the contribution of colleagues from Faculty of Resource Science and Technology (FRST) Geochemistry Laboratory and Analytical Laboratory, Universiti Malaysia Sarawak. This research was supported by Universiti Malaysia Sarawak, Tun Openg Chair, with Research Grant Code: F07/TOC/1738/2018.

REFERENCES

1. Nanomaterials state of the market Q3 2008: Stealth Success, broad impact. Lux Research, 2008. Lux Research Inc New York.
2. Sargent, J. F., “Nanotechnology: A Policy Primer”, Congressional Research Service, 2016. http://eprints.internano.org/id/eprint/2357.
3. Federici, G., Shaw, B. J., and Handy, R. R., “Toxicity of Titanium Dioxide Nanoparticles to Rainbow Trout (Oncorhynchus mykiss): Gill Injury, Oxidative Stress, and Other Physiological Effects”, Aquatic Toxicology, 2007, 84, 415-430.
4. Liu, H., Ma, L., Zhao, J., Liu, J., Yan, J., and Ruan, J., Hong, F., “Biochemical Toxicity of Nano-anatase TiO_2 Particles in Mice”, Biological Trace Element Research, 2009, 129 (1-3), 170-180.
5. Nel, A., Xia, T., Madler, L., and Li, N., “Toxic Potential of Materials at the Nanolevel”, Science, 2006, 311(5761), 622-627.
6. Mortensen, L. J., Oberdorster, G., Pentland, A. P., and Delouise, L. A., “In Vivo Skin Penetration of Quantum Dot Nanoparticles in the Murine Model: The effect of UVR”, Nano Letters, 2008, 8 (9), 2779-2787.
7. Piccinno, F., Gottschalk, F., Seeger, S., and Nowack, B., “Industrial production quantities and uses of ten engineered nanomaterials for Europe and the world”, J. Nanopart. Res. 2012, 14, 1109–1120.

[DOI: 10.22068/ijmse.17.4.152]

8. Handy, R. D., Kammer, F. V. D., Lead, J. R., Hassello ¨v, M., Owen, R., and Crane, M., "The ecotoxicity and chemistry of manufactured nanoparticles", Ecotoxicology, 2008, 17, 287–314.
9. Nowack, B., "The behavior and effects of nanoparticles in the environment", Environmental Pollution, 2009, 157, 1063–1064.
10. Kahru, A., Ivask, A., Kasemets, K., Pollumaa, L., Kurvet, I., Francois, M., and Dubourguier, H-C., "Biotests and biosensors in ecotoxicological risk assessment of field soils polluted with zinc, lead and cadmium", Environmental Toxicology and Chemistry: An International Journal, 2005, 24(11), 2973-2982.
11. Lock, K., and Janssen, C. R., "Comparative toxicity of zinc salt, zinc powder and zinc oxide to Eisenia, fetida, Enchytraeus albidus and Folsomia candida", Chemosphere, 2003, 53 (8), 851–856.
12. Piao, F., Yokoyama, K., Ma, N., and Yamauchi, T., "Subacute toxic effects of zinc on various tissues and organs of rats", Toxicol. Lett. 2003, 145 (1), 28–35.
13. Gottschalk, F., Kost, E., and Nowack, B., "Engineered nanomaterials in water and soils: a risk quantification based on probalistic exposure and effect modelling", Environ. Toxicol. 2013, Chem. 32(6), 1278-1287.
14. Wang, X. S., Li, Z. Z., and Tao, S. R., "Removal of chromium (VI) from aqueous solution using walnut hull", Journal of Environmental Management, 2009, 90(2), 721-729.
15. Vijayalakshmi, K., Devi, B. M., Latha, S., Gomathi, T., Sudha, P. N., Venkatesan, J., and Anil, S., "Batch adsorption and desorption studies on the removal of lead (II) from aqueous solution using nanochitosan/sodium alginate/microcrystalline cellulose beads", International Journal of Biological Macromolecules, 2017, S0141-8130(16) 32016-5.
16. Aslam, M., Rais, S., Alam, M. and Pugazhendi, A. "Adsorption of Hg(II) from Aqueous Solution Using Adulsa (Justicia adhatoda) Leaves Powder: Kinetic and Equilibrium Studies", Journal of Chemistry, 2013, ArticleID174807,1-11.
17. Wahi, R., Kanakaraju, D., and Yusuf, N. A., "Preliminary Study on Zinc Removal from Aqueous Solution by Sago Wastes", Global Journal of Environmental Research, 2010, 4 (2), 127-134.
18. Hiroshi, E., Yukio, T., and Dennis, V. J., "Sago Palm: multiple contributions to food security and sustainable livelihoods", Published by Springer Nature, 2018, 11-13.
19. Amin, N., Sabli, N., Izhar, S., and Yoshida, H., "Sago Wastes and Its Applications", Pertanika J. Sci. & Technol., 2019, 27(4), 1841-1862.
20. Singhal, R. S., Kennedy, J. F., Gopalakrishnan, S. M., Kaczmarek, A., Knill, C. J., and Akmar, P. F., "Industrial Production, Processing and Utilization of Sago Palm-derived Products", Carbohydrate Polymer, 2008, 72: 1-20.
21. Wahi, R., Luqman, C. A., Mohsen, N. M., Ngaini, Z., and Thomas, C. S. Y., "Utilization of esterified sago bark fibre waste for removal of oil from palm oil effluent", Journal of environmental chemical engineering, 2017, 5, 170-177.
22. Droepenu, E. K., Asare, E. A., "Morphology of green synthesized ZnO nanoparticles using low temperature hydrothermal technique from aqueous Carica papaya extract", Nanoscience and Nanotechnology, 2019, 9 (1), 29-36.
23. Droepenu, E. K., Boon, S. W., Chin, S. F., Kuan, Y. K., Zaini, B. A., and Asare, E. A., "Comparative evaluation of antibacterial efficacy of biological synthesis of ZnO nanoparticles using fresh leaf extract and fresh stem bark of Carica papaya", Nano Biomed. Eng. 2019, 11 (3), 264-271.
24. Droepenu, E. K., Asare, E. A., Dampare, S. B., Adotey, D. K., Gyampoh, A. O., and Kumi-Arhin, E., "Laboratory and Commercial Synthesized Zinc Oxide Nanoparticles Adsorption onto Coconut Husk: Characterization, Isotherm, Kinetic, and Thermodynamic Studies", Biointerface Research in Applied Chemistry, 2021, 11(1), 7871-7889.
25. Zhou, M., Wei, Z., Qiao, H., Zhu, L., Yang, H., and Xia, T., "Particle size and pore structure characterization of silver nanoparticles prepared by confined arc plasma", J. Nanomater, 2009, 1-5. http://doi:10.1155/2009/968058.

[DOI: 10.22068/ijmse.17.4.152]

26. Langmuir, I., "The constitution and fundamental properties of solids and liquids", J. Am. Chem. Soc., 1916, 38(11), 2221-2295.
27. Webber, T. W., and Chakkravorti, R. K., "Pore and solid diffusion models for fixed bed adsorbers", AIChE J. 1974, 20, 228-238.
28. Freundlich, H. M. F., "Over the adsorption in solution", J. Phys. Chem., 1906, 57, 385-471.
29. Temkin, M. I., and Pyzhev, V., "Kinetics of ammonia synthesis on promoted iron catalyst", Acta Phys. Chim., USSR, 1940, 12, 327-356.
30. Akkaya, G., and Ozer, A., "Adsorption of acid red 274 (AR 274) on Dicranella varia: Determination of equilibrium and kinetic model parameters", Process Biochem, 2005, 40, 3559–3568.
31. Pearce, C. I., Lloyd, J. R., and Guthrie, J. T., "The removal of colour from textile wastewater using whole bacterial cells: A review", Dyes Pigments, 2003, 58, 179–196.
32. Lakshmipathy, R., and Sarada, N. C., "Methylene blue adsorption onto native watermelon rind: batch and fixed bed column studies", Desalin. Water. Treat. 2016, 57(23), 10632-45.
33. Zareie, C., Najafpoura, G., and Baei, M. S., "Preparation of nanochitosan as an effective sorbent for the removal of copper ions from aqueous solutions", IJE Transac. B: Appl. 2013, 26, 829-836.
34. Rao, M. M., Ready, D. D. K. K., Venkateswarl, P., and Seshaiah, K., "Removal of mercury from aqueous solution using activated carbon prepared from agriculture by-product/waste", J. Environmental Management, 2008, 90(1):634-643.
35. Lim, T. T., and Huang, X., "Evaluation of hydrophobicity/oleophilicity of kapok and its performance in oily water filtration: comparison of raw and solvent-treated fibers", Ind. Crops Prod., 2007, 26, 125–134.
36. Tserki, V., Zafeiropoulos, N. E., Simon, F., and Panayiotou, C., "A study on the effect of acetylation and propionylation surface treatments on natural fibers", Compos. A: Appl. Sci. Manuf. 2005, 36, 1110–1118.
37. Adebajo, M. O., and Frost, R. L., "Infra-red and 13-C MAS nuclear magnetic resonance spectroscopic study of acetylation of cotton", Spectrochim. Acta A, 2004, 60, 449–453.
38. Banerjee, M., Basu, R.K., and Das, S.K., "Cr(VI) adsorption by a green adsorbent walnut shell: adsorption studies, regeneration studies, scale-up design and economic feasibility", Process Safety and Environment Protection, 2018, 116, 693-702.
39. Kanthasamy, S., Hadibarata, T., Hidayat, T., Alamri, S. A., and Al-Ghamdi, A. A., "Adsorption of azo and anthraquinone dye by using watermelon peel powder and corn peel powder: equilibrium and kinetic studies", Biointerface Research in Applied Chemistry, 2020, 10(1), 4706 – 4713.
40. Malik, R., Ramteke, D., and Wate, S.R., 2006 "Physico-chemical and surface characterization of adsorbent prepared from groundnut shell by $ZnCl_2$ activation and its ability to absorb colour". Indian Journal of Chemical Technology, 13(4), 319-328.
41. Zhang, X., and Wang, X., "Adsorption and Desorption of Nickel (II) Ions from Aqueous Solution by a Lignocellulose/ Montmorillonite Nanocomposite", PLoS ONE, 2015, 10(2), 1-21.
42. Makeswari, M., Santhi, T., Aswini, P. K., "Adsorption of nickel ions by using binary metal oxides from aqueous solution", Int. J. Adv. Res., 2016, 4, 542-553.
43. Putra, W. P., Kamari, A., Yusoff, S. N. M., Ishak, C. F., Mohamed, A., Hashim, N., and Isa, I.Md., "Biosorption of Cu(II), Pb(II) and Zn(II) ions from aqueous solutions using selected waste materials: Adsorption and characterisation studies", J. Encapsul. Adsorp. Sci., 2014, 4, 25-35.
44. Bhatti, H. N., Mumtaz, B., Muhammad, A. H., and Nadeem, R., "Removal of Zn (II) ions from aqueous solution using Moringa oleifera Lam (Horseradish Tree) biomass", Process Biochemistry, 2007, 42: 547-553.
45. Velintine, V. A., Wee, B. S., Chin, S. F., and Kok, K. Y., "Transformation of zinc oxide nanoparticles under environmentally relevant conditions: influence of pH and ionic strength", Transactions on Science and Technology, 2017, 4(2), 123-136.
46. Piplai, T., Kumar, A., and Alappat, B. J., "Removal of mixture of ZnO and CuO nanoparticles (NPs) from water using activated carbon in batch kinetic studies", Water Science & Technology, 2017, 75.4, 1-21.

[DOI: 10.22068/ijmse.17.4.152]

47. Chandrasekaran, T., Arunkumar, A., and RiazAhamed, K., "Removal of Pb (II) ions from aqueous solutions using activated carbon prepared from plant Glycosmis mauritiana", J. Chem. Pharm. Res. 2016, 8, 704-711.
48. Al-Jariri, J. S., and Khalili, F., "Adsorption of Zn(II), Pb(II), Cr(III) and Mn(II) from water by Jordanian Bentonite", Desalin. Water. Treat., 2012, 21, 308-322.
49. Reddy, D., Seshaiah, K., Reddy, A. V. R., and Lee, S. M., "Optimization of Cd(II), Cu(II) and Ni(II) biosorption by chemically modified Moringa oleifera leaves powder", Carbohydr. Polym., 2010, 88, 1077-1086.
50. Harikumar, P. S., and Anisha Aravind, B. P., "Heavy metal removal from waste water using Copper alumina Nanocomposite", Int. J. Innov. Appl. Res., 2016, 4, 35- 44.
51. Abdel-Ghani, N. T., Hefny, M., and El-Chaghaby, G. A. F., "Removal of lead from aqueous solution using low cost abundantly available adsorbents", Int. J. Environ. Sci. Tech., 2007, 4(1), 67–73.
52. Bishnoi, N. R., "Biosorption of Cu (II) from aqueous solution using algal biomass", J. Sci. Ind. Res., 2004, 63, 813–816.
53. Gong, R., Ding, Y., Liu, H., Chen, Q., and Liu, Z., "Lead biosorption and desorption by intact and pretreated spirulina maxima biomass", Chemosphere, 2005, 58 (1), 125–30.
54. Saifuddin, N., and Raziah, A. Z., "Removal of heavy metals from industrial effluent using Saccharomyces cerevisiae (Baker's yeast) immobilized in chitosan / lignosulphonate matrix", Journal of Applied Science Research, 2007, 3, 2091–2099.
55. Aydin, H., Bulut, Y., and Yerlikaya, C., "Removal of copper (II) from aqueous solution by adsorption onto low-cost adsorbents", J. Environmental Management, 2008, 87, 37-5.
56. Akar, S. T., Ozcan, A. S., Akar, T., Ozcan, A., and Kaynak, Z., "Biosorption of a reactive textile dye from aqueous solutions utilizing an agrowaste", Desalination, 2009, 249(2), 757–761.
57. Srivastava, V. C., Mall, I. D., and Mishra, I. M., "Characterization of mesoporous rice husk ash (RHA) and adsorption kinetics of metal ions from aqueous solution onto RHA", J. Hazard. Mater. B, 2006, 134, 257.
58. Deepa, C. N., and Suresha, S., "Biosorption of Ni(II) in aqueous solution and industrial wastewater by leaves of Araucaria cookie", Int. J. Res. Chem. Environ., 2014, 4, 101-108.
59. Lakherwal, D., Rattan, V. K., and Singh, H. P., "Studies on adsorption of nickel by activated carbon in a liquid fluidised bed reactor", Canadian. Chem. Trans., 2016, 4, 121-132.
60. Zhang, P., Ding, W., Zhang, Y., Dai, K., and Liu, W., "Heavy metal ions removal from water using modified zeolite", J. Chem. Pharm. Res., 2014, 6, 507-514.
61. Ozer, A., and Ozer, D., "Comparative study of the biosorption of Pb (II), Ni (II) and Cr (VI) ions onto S. cerevisiae: determination of biosorption heats", J. Hazard Mater., 2003, 100, 219–229.
62. Rajakovic-Ognjanovic, V., Aleksic, G., and Rajakovic, Lj., "Governing factors for motor oil removal from water with different sorption materials", J. Hazard. Mater., 2007, 154(1-3), 558-563.
63. Kumar, D., Pandey, K., and Gaur, P., "Evaluation of various isotherm models, and metal sorption potential of cyanobacterial mats in single and multi-metal systems", Colloids and Surfaces B: Journal of Biointerfaces, 2010, 81(2), 476-485.
64. Quek, S. Y., Wase, D. A. J., and Forster, C. F., "The use of sago waste for the sorption of lead and copper", Water Sa., 1998, 24(3), 251-256.
65. Wahi, R., Luqman, C. A., Mohsen, N. M., Ngaini, Z., and Thomas, C. S. Y., "Utilization of esterified sago bark fibre waste for removal of oil from palm oil mill effluent", Journal of Environmental Chemical Engineering, 2016, 5, 170–177.
66. Maheswari, P., Venilamani, N., Madhavakrishnan, S., Shabudeen, P. S. S., Venckatesh, R., and Pattabhi, S., "Utilization of Sago Waste as an Adsorbent for the Removal of Cu(II) Ion from Aqueous Solution", E-Journal of Chemistry, 2008, 5(2), 233-242.
67. Wahi, R., Kanakaraju, D., and Yusuf, N. A., "Preliminary Study on Zinc Removal from Aqueous Solution by Sago Wastes". Global Journal of Environmental Research 4 (2): 127-134, 2010.

[DOI: 10.22068/ijmse.17.4.152]